Assessment of CHF Enhancement Mechanisms in a Curved, Rectangular Channel Subjected to Concave Heating

J. C. Sturgis
Graduate Student

I. Mudawar[1]
Professor and Director,
Fellow ASME

Boiling and Two-Phase Flow Laboratory,
School of Mechanical Engineering,
Purdue University,
West Lafayette, IN 47907

An experimental study was undertaken to examine the enhancement in critical heat flux (CHF) provided by streamwise curvature. Curved and straight rectangular flow channels were fabricated with identical 5.0 × 2.5 mm cross sections and heated lengths of 101.6 mm in which the heat was applied to only one wall—the concave wall (32.3 mm radius) in the curved channel and a side wall in the straight. Tests were conducted using FC-72 liquid with mean inlet velocity and outlet subcooling of 0.25 to 10 m s^{-1} and 3 to 29°C, respectively. Centripetal acceleration for curved flow reached 315 times earth's gravitational acceleration. Critical heat flux was enhanced due to flow curvature at all conditions but the enhancement decreased with increasing subcooling. For near-saturated conditions, the enhancement was approximately 60 percent while for highly subcooled flow it was only 20 percent. The causes for the enhancement were identified as (1) increased pressure on the liquid-vapor interface at wetting fronts, (2) buoyancy forces and (3) increased subcooling at the concave wall. Flow visualization tests were conducted in transparent channels to explore the role of buoyancy forces in enhancing the critical heat flux. These forces were observed to remove vapor from the concave wall and distribute it throughout the cross section. Vapor removal was only effective at near-saturated conditions, yielding the observed substantial enhancement in CHF relative to the straight channel.

Introduction

Critical heat flux represents a thermal limit that if surpassed can result in destructive failure of a device. Since many modern devices operate at high heat fluxes, it is desirable to increase this limit permitting both a broader heat transfer operating range and a larger margin of safety. Applications which may benefit from such an increase are direct-immersion cooling of electronic components, nuclear reactor cooling, transfer of solar energy to a working fluid, and rocket engine combustion chamber cooling. One means for enhancing CHF in flow boiling is streamwise curvature. Of particular interest to the present study are curved, rectangular passages subjected only to concave heating since this configuration isolates the enhancement effect. Realizing the drastic consequences of surpassing the CHF limit and the implications of raising it, the present authors sought to examine this enhancement effect through both heat transfer measurements and flow visualization.

Streamwise curvature has been shown to enhance both single and two-phase heat transfer. Hughes and Olson (1975) performed flow boiling tests in one-side-heated rectangular channels using thin, ribbon heaters. For heating along the entire 180-deg turn of the concave wall, they measured an enhancement in CHF compared to a straight wall for highly subcooled flow (28–61°C). Wu and Simon (1995) conducted tests with a thin, low thermal-capacitance platinum surface located at 90 deg along the concave wall. With this localized heater, they recorded CHF enhancements that decreased with increasing subcooling. Wu and Simon (1994) performed similar tests with a thick copper-bar heater which provided a boiling surface extending over only a portion of the channel width. Galloway and Mudawar (1995) used a thick but short copper heater which provided heat to the entire width of the concave wall over a short length centered at 135 deg into the turn. Their tests at near-saturated conditions and low velocities yielded an average CHF enhancement of 23 percent.

The results of these investigators are closely related to the conditions under which the experiments were conducted. For example, heated length is known to affect CHF. Vapor generated on upstream regions of long heaters coalesces downstream impeding the movement of cooler bulk liquid toward the surface. The vapor layer is not as thick on short localized heaters operating at the same heat flux. Gersey and Mudawar (1995a) showed that CHF decreases with increasing heated length for the same inlet conditions.

Secondly, the thermal mass of the heater influences surface boiling. Ribbon heaters (0.08–0.13-mm thick nichrome (Hughes and Olson (1975)) and sputtered boiling surfaces (800-Å thick platinum (Wu and Simon (1995)) are more susceptible to imperfections which could lead to local hot spots and the coexistence of different heat transfer regimes on the surface. A thick heater would not support this behavior since heat would be conducted to locations of least resistance.

Thirdly, the cross-sectional geometry of the heated section affects coalescence. Vapor generated from a localized heater that does not extend the full width of the channel is not as confined by the side walls as vapor from a full-width heater. Coalescence also depends on whether the shorter or longer dimension of a high aspect ratio channel is heated.

Additionally, there is disagreement regarding the effects of subcooling and centripetal acceleration on CHF enhancement. The generally reported trend is one of decreasing enhancement with increasing subcooling. Leland and Chow (1992) even measured a detrimental curvature effect for highly subcooled flow though many other researchers did not. Gambill and Green (1958) and Gu

[1] To whom correspondence should be addressed. e-mail: mudawar@ecn.purdue.edu.

Contributed by the Heat Transfer Division for publication in the JOURNAL OF HEAT TRANSFER. Manuscript received by the Heat Transfer Division, Feb. 13, 1998; revision received, Jan. 15, 1999. Keywords: Boiling, Enhancement, Experimental, Forced Convection, Heat Transfer, Visualization. Associate Technical Editor: P. Ayyaswamy.

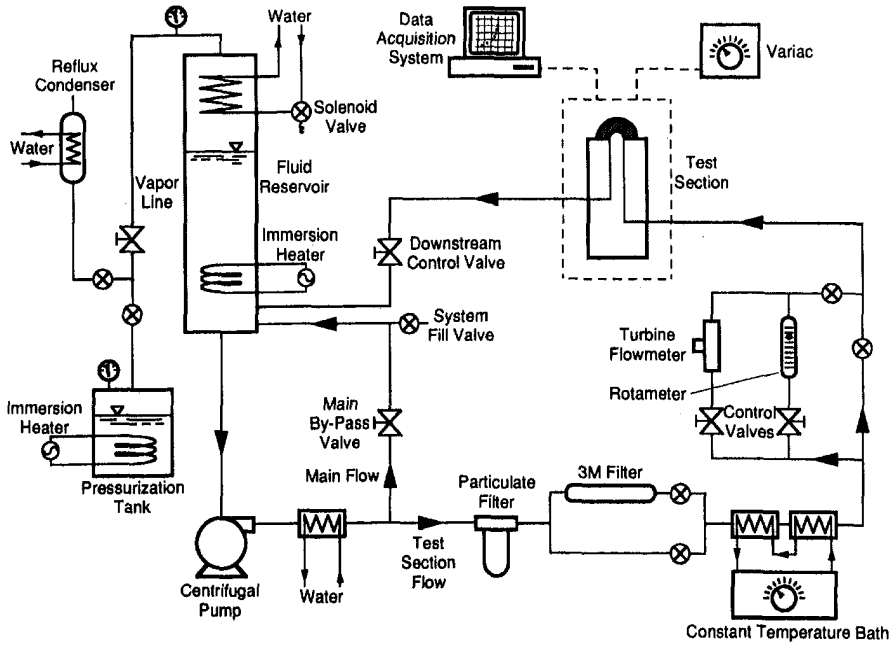

Fig. 1 Closed two-phase flow loop and auxiliary components

et al. (1989) correlated their respective enhancement factors with centripetal acceleration to the one-fourth power, drawing on the pool boiling correlation proposed by Zuber et al. (1961) which contained earth's gravity to the $\frac{1}{4}$-power. This dependence of CHF on centripetal acceleration remains inconclusive requiring further rigorous evaluation.

The limitations of these prior studies point to a need to more systematically explore the enhancement mechanisms using both CHF data and flow visualization. The present experimental study was set up to obtain CHF data for near-saturated and subcooled flow in a curved, rectangular channel subjected only to concave heating using a long thick heater. The same test matrix, which included a broad range of velocity, was repeated for a straight channel in order to assess the enhancement for which curvature is responsible. In this manner, the curvature enhancement effect could be isolated and quantified. Additionally, flow visualization tests were conducted to gain insight into the mechanisms responsible for the enhancement indicated in the data.

Experimental Methods

Flow Loop. Heat transfer experiments were conducted using a closed two-phase flow loop, a schematic of which is shown in Fig. 1. It consisted of a large cylindrical reservoir, centrifugal pump, flat-plate heat exchangers, flow control valves, flowmeters, test section, and CPVC piping. The fluid selected for this investigation was FC-72, a dielectric Fluorinert manufactured by 3M Company. Its main attributes are a low boiling point (57°C at 1 atm) and a relatively low heat of vaporization, allowing for only a modest heat input to achieve boiling.

Nomenclature

C_1, C_2 = constants in Eq. (1)
C_3, C_4 = constants in Eq. (2)
d_{up} = measured distance from heater inlet to upstream edge of vapor patch
D_h = hydraulic diameter of channel
g^* = centripetal acceleration nondimensionalized with respect to g_e
g_c = centripetal acceleration
g_e = earth's gravitational acceleration
h = change in position along an acceleration vector
l_{meas} = measured liquid length between vapor patches
P_o = fluid pressure at outlet of heated section
P_{2c} = pressure at concave wall of curved channel
P_{2s} = pressure throughout cross section of straight channel
ΔP = radial pressure rise in curved channel
q'' = heat flux
q''_m = maximum nucleate boiling heat flux, CHF
r = radial coordinate in curved heater
R_1 = radius of inner wall of curved channel
R_2 = radius of outer wall of curved channel
Re_D = Reynolds number, UD_h/ν_f
T = temperature
T_b = fluid bulk temperature
T_o = fluid temperature at outlet of heated section
$T_{sat,o}$ = fluid saturation temperature (at P_o) at outlet of heated section
T_w = wall temperature
$\Delta T_{sub,o}$ = fluid subcooling at outlet of heated section at CHF
U = mean inlet velocity
x = transverse coordinate in straight heater, $x = 0$ at fluid-surface interface
z = streamwise coordinate, $z = 0$ at heater inlet

Greek

δ_{meas} = measured vapor patch height
λ_{meas} = measured vapor patch length
ρ = density
ν = kinematic viscosity

Subscripts

cur = curved channel/heater
f = liquid
o = outlet of heated section
sat = saturated
str = straight channel/heater

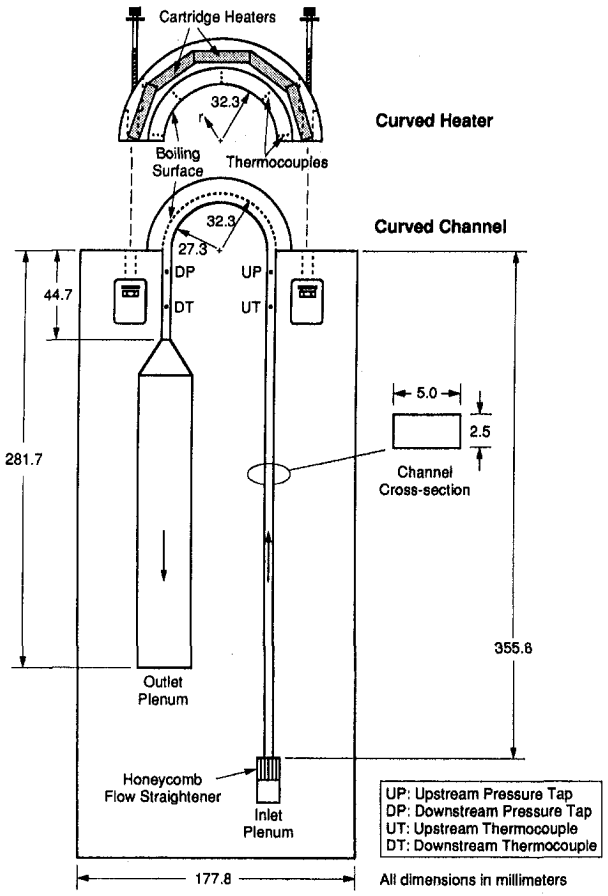

Fig. 2 Curved heater and bottom plate of curved channel

Fluid temperature was controlled by an immersion heater submerged in the reservoir and by a series of flat-plate heat exchangers. System pressure could be adjusted by the addition of FC vapor into the reservoir which was generated in a pressurization tank.

Test Channels. Two channel designs were tested in this investigation—a curved and a straight channel, shown in Figs. 2 and 3, respectively. Nearly identical except for the curvature of the heated section, they had the same cross section (5.0 × 2.5 mm), hydrodynamic entry length (106 hydraulic diameters), heated length (101.6 mm), flow instrumentation, and material.

Each channel was fabricated from two plates of opaque high-temperature G-10 fiberglass plastic. In the bottom plate of each channel (shown in Figs. 2 and 3) was machined a groove that had the width and depth of the channel. This groove had three surfaces except at the heater location where one of the walls had been removed. The heater was installed in this location and aligned with the aid of a microscope flush with the interrupted wall. In this manner, the flow channel remained rectangular with smooth, continuous walls—one of which contained a 101.6-mm long heated segment. In the curved channel, this heated segment was the concave wall whereas in the straight channel it was a side wall. When the second plate of G-10 fiberglass plastic was placed on top, it closed out the channel, forming the fourth wall. A flexible Teflon cord placed in a shallow O-ring groove on the underside of the top piece sealed the channel when the two G-10 plates and copper heater were bolted together. Flow channel instrumentation consisted of upstream and downstream thermocouples and pressure transducers as indicated in Figs. 2 and 3.

Copper Heaters. Two heaters were fabricated for testing, one curved, Fig. 4(*a*), and the other straight, Fig. 4(*b*). They were made from 99.99 percent pure oxygen-free copper and were identical in most respects except for the curvature. For each, the heated surface exposed to the flow measured 2.5 mm in width and 101.6 mm along the flow direction.

Three Type-K thermocouples were placed at each of five locations along the heaters to determine the local heat flux and wall temperature, with corresponding locations the same distance from the inlet in both the curved and straight heaters. These thermocouples are indicated in Fig. 4, with Locations 1 and 5 referring to the inlet and outlet sets, respectively. The three small holes at each location were precisely drilled with respect to each other and the heated wall. Thermocouple beads (0.33-mm diameter) were inserted into these holes then secured in place with high conductivity epoxy.

Power was supplied by cylindrical cartridge heaters connected to a 240-volt variac and embedded in the thick portions of the curved and straight heaters as shown in Figs. 2 and 3, respectively. Distributing cartridge heaters as shown and using a high conductivity material for both heaters ensured power was evenly applied along the beginning of the thin portion. Heat then flowed through this thin portion toward the fluid resulting in a temperature gradient measured by the thermocouples.

Data Reduction. The component of flux perpendicular to the channel wall was approximated from the temperature gradient in the same direction. The three thermocouple readings were used in a one-dimensional analysis to determine this average flux for the corresponding instrumented location. This was accomplished using a linear-squares best-fit solution to first calculate the logarithmic profile in the curved heater or linear profile in the straight heater, which are given, respectively, by

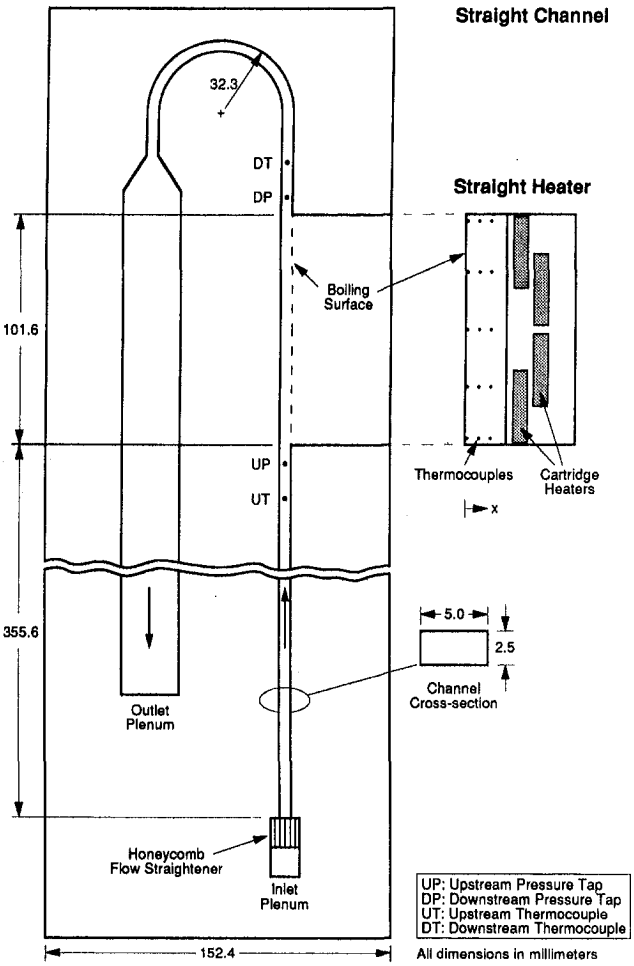

Fig. 3 Straight heater and bottom plate of straight channel

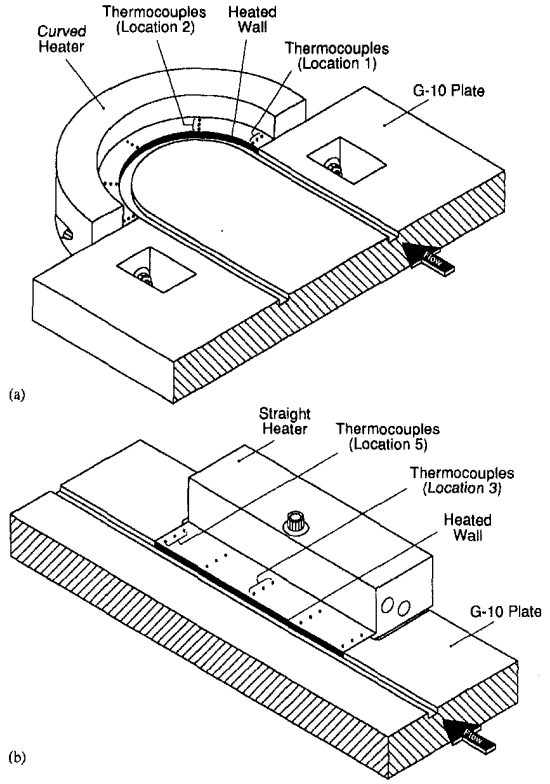

Fig. 4 (*a*) Curved and (*b*) straight heaters inserted into their respective channels with the five thermocouple locations in each heater shown

$$T(r) = C_1 \ln\left(\frac{r}{R_2}\right) + C_2 \tag{1}$$

and

$$T(x) = C_3 x + C_4, \tag{2}$$

where $r = R_2$ indicates the concave surface and $x = 0$ the straight surface. With the profile established, calculations of wall heat flux, q'', and wall temperature, T_w, at a given location were straightforward, with a constant copper conductivity of 391 W m^{-1} K^{-1} assumed. The consequences of calculating a slope and extrapolating a value from a profile that was based on discrete data points were minimized by using a best-fit solution and by averaging temperature readings over 14 seconds while at steady-state conditions.

The calculations of bulk fluid temperature, T_b, at each location and outlet temperature, T_o, were based on heat input up to the respective locations and the assumption of a well-mixed flow. Since it is difficult to measure temperature when vapor exists in a subcooled liquid, the bulk average temperature (i.e., thermodynamic equilibrium temperature) is calculated in order to be able to plot a boiling curve and compare data.

The critical heat flux, q''_m, was defined as the largest flux attained under steady conditions. Since at CHF a vapor blanket essentially insulates the surface, heat supplied by the cartridge heaters could no longer be removed by the liquid and remained in the copper to cause a temperature rise and gradient decrease. Hence, CHF was detected by observing the data for an unsteady increase in calculated wall temperature accompanied by a sudden decrease in calculated wall flux. Since power increments were small, the flux prior to this unsteady behavior was recorded as the critical heat flux.

Test Conditions. Fluid in the loop was deaerated prior to each series of tests. Once inlet temperature, outlet pressure and flow rate were adjusted to desired values, power to the heater was incremented. A data point was recorded at each power setting after thermal conditions were deemed steady. Each test proceeded through single and two-phase heat transfer regimes generating a boiling curve which terminated immediately after critical heat flux.

These heat transfer tests were conducted at three outlet subcoolings ($\Delta T_{sub,o} = T_{sat,o} - T_o = 3$, *16,* and 29°C) with 13 flow velocities ($U = 0.25$ to 10 m s^{-1}) examined at each subcooling. $\Delta T_{sub,o}$ refers to the prevailing subcooling value at the outlet of the heated section at the time of critical heat flux. Since the outlet pressure was held constant at $P_o = 1.38$ bar for all tests, the prevailing FC-72 saturation temperature at the outlet remained constant ($T_{sat,o} = 66.3$°C) as well. Therefore, at the time of critical heat flux, the outlet fluid bulk temperature achieved a prescribed value ($T_o = 63.3$, 50.3 or 37.3°C) depending on the subcooling value desired for that test. The inlet temperature remained constant during a particular test and was chosen such that the outlet temperature would equal its desired value at CHF. Maintaining a constant outlet pressure for all tests as well as a constant outlet temperature (at CHF) for tests with the same subcooling allowed for a meaningful comparison of CHF data.

For the velocity range tested, the Reynolds number based on hydraulic diameter and inlet conditions, $\mathrm{Re}_D = UD_h/\nu_f$, ranged from 2,000 to 130,000. Considering also that the hydrodynamic entry length measured over 100 hydraulic diameters, fully developed turbulent flow was assumed to exist at the heater inlet. Correspondingly, centripetal acceleration, defined as

$$g^* = \frac{U^2}{R_2 g_e}, \tag{3}$$

ranged from 0 to 315. Though T_{in} remained constant for a given test, it had to be increased as test velocity increased, such that it varied over the ranges of 48 to 62, 32 to 49 and 17 to 35°C corresponding to outlet subcooling values of 3, 16 and 29°C, respectively.

Earth's gravity had a negligible effect on the flow even at low velocities due to the small channel width and the orientation of the gravity vector parallel to the heated surface and perpendicular to the bulk motion.

Repeatability and Uncertainty Analysis. The procedures for assembling the channel and acquiring data were consistent throughout the test program. Boiling curves for duplicated tests were nearly identical indicating repeatable results, negligible aging of the channel and consistent assembly procedures. For multiple tests at the same test condition, CHF values differed from their average by less than 3.4 percent. This is within the uncertainty in heat flux, which is approximately 8.5 percent at low fluxes ($q'' \approx 300$ kW m^{-2}) decreasing to less than five percent at high fluxes ($q'' \approx 1500$ kW m^{-2}). Uncertainty in calculated flux arose from uncertainties in temperature differences among the three thermocouples, thermocouple spacing and copper conductivity. The latter two uncertainties were assumed constant while the former decreased in significance as magnitude of temperature difference (i.e. flux) increased. Wall temperature calculations were accurate to within 0.3°C and flow rate uncertainty was less than 2.3 percent.

Numerical modeling revealed that heat losses from the thin, instrumented portion of the heater represented only about five percent of the heat flowing into this segment for low fluxes ($q'' \approx$ 150 kW m^{-2}) and decreased for higher fluxes. Using low conductivity (0.26 W m^{-1} K^{-1}) G-10 channel plates, high conductivity copper for the heater, and a short span for the thin instrumented portion helped minimize the heat losses, which were neglected in calculations.

Experimental Results

The CHF values measured in the present study are given in Tables 1 and 2 for the straight and curved channels, respectively. In both cases, CHF increased with increasing velocity and increas-

Table 1 Critical heat flux data for the straight channel

U (m s^{-1})	0.25	0.5	1.0	1.5	2	3	4	5	6	7	8	9	10
$\Delta T_{sub,o}$ (°C)													
3	240 [a]	251	282	305	313	343	368	365	378	423	469	529 [b]	628 [c]
	250	249			329	348		365					
						347							
16	318 [a]	352	388	418	443	470	524	631	717	766	858	937	1025
	319	355	383	420	440		518		693	764			1036
					428								
29	389 [a]	427	488	540	594	707	869	971	1087	1182	1293	1416	1526
	394	431	484	515		736							
				512									

CHF values in kW m^{-2}; a: $\Delta T_{sub,o}$ is more than 1 °C below nominal value; b: $\Delta T_{sub,o} = 4$ °C; c: $\Delta T_{sub,o} = 5$ °C.

ing subcooling. The increase associated with subcooling is due to the cooler bulk temperature more readily condensing the bubbles before they coalesce into a vapor blanket. This relationship was linear in the straight channel as shown in Fig. 5, a result supported by the work of Wu and Simon (1994) and Collier and Thome (1994). However, CHF in the curved channel did not display a consistently linear relationship with subcooling over the same range of velocity. One reason for this inconsistency, which will become more apparent later, concerns the different influence buoyancy forces have on vapor removal from the concave wall for highly subcooled conditions as compared to near-saturated conditions.

The comparison of straight and curved-channel boiling curves in Fig. 6 reveals the enhancement of both single and two-phase heat transfer that streamwise curvature provides. Shown are increases in the single-phase convection coefficient, the incipient boiling heat flux and the critical heat flux. For $\Delta T_{sub,o} = 29$°C, Fig. 6 shows the enhancement in CHF decreases with increasing velocity—from 48 percent at $U = 2$ m s^{-1} to 20 percent at $U = 10$ m s^{-1}.

Figure 7 shows CHF data for the curved channel normalized relative to those for the straight channel in the form of enhancement ratios. The x-axis shows flow velocity on a linear scale along with the nondimensional centripetal acceleration, g^*. In most cases, the lowest subcooling, $\Delta T_{sub,o} = 3$°C, offered the largest enhancement ratio and for $U > 2$ m s^{-1} this was between 60 and 70 percent. At the low end of the velocity range, the middle and high subcooling values alternated in offering the better enhancement due in part to the fact that at some of these velocities CHF was detected at different locations along the heater. At higher velocities, where CHF was detected solely at the outlet, the CHF enhancement ratios tended toward constant values, approximately 60 percent for $\Delta T_{sub,o} = 3$°C, 40 percent for $\Delta T_{sub,o} = 16$°C and 20 percent for $\Delta T_{sub,o} = 29$°C.

The CHF enhancement ratio, but not CHF, decreased with increasing subcooling. Hughes and Olson (1975) recorded similar trends for the curvature enhancement effect. They performed tests with Freon-113 for velocities of 1 to 4 m s^{-1} for highly subcooled flow (28–61°C) in rectangular channels in which heat was applied to the straight, convex, or concave wall. Their data also showed the concave-to-straight-channel CHF ratio decreased with increasing subcooling. Gu et al. (1989) reported CHF enhancement of greater than 40 percent for FC-72 at $U = 4$ m s^{-1} at both low (0.5°C) and moderate (20°C) subcooling. However, at $U = 1$ m s^{-1}, the curvature enhancement dropped as subcooling increased. Wu and Simon (1994) also noted the tendency for the curved-to-straight CHF ratio to diminish with increasing subcooling, as did Leland and Chow (1992) who actually reported a detrimental curvature effect for 35°C subcooling in their smaller radius ($R_2 = 28.6$ mm) channel.

The solid curve in Fig. 7 represents the curvature enhancement ratio if it were a function of centripetal acceleration to the one-fourth power. Several researchers (Gambill and Green, 1958; Gu et al., 1989), following the work of Zuber et al. (1961), have proposed this relationship for CHF in curved channels. Zuber et al. offered a correlation for *pool boiling* in which CHF is proportional to earth's gravitational acceleration, g_e, to the $\frac{1}{4}$-power. Researchers have sought to extend this dependence to curved flow by replacing g_e with the local centripetal acceleration resulting in a CHF ratio dependent on g^* to the one-fourth power. This relation is not reflected by the CHF data obtained for the wide ranges of velocity and subcooling in the present investigation. The radial pressure gradient in curved flow must therefore be responsible for

Table 2 Critical heat flux data for the curved channel

U (m s^{-1})	0.25	0.5	1.0	1.5	2	3	4	5	6	7	8	9	10
g^*	0	1	3	7	13	28	50	79	114	154	202	255	315
$\Delta T_{sub,o}$ (°C)													
3	370	411	436	473	435	559	586	598	651	695	757	863 [b]	1006 [c]
	374	413	443	472	481		582	620			759		
					482								
16	444	509	570	660	570	634	701	791	883	998	1156	1267	1438
	445	507	560	671			739						1436
				657									
29	470 [a]	578	683	804	880	1021	1158	1309	1376	1446	1562	1673	1825
	467	580	673	787	874			1277					

CHF values in kW m^{-2}; a: $\Delta T_{sub,o}$ is more than 1 °C below nominal value; b: $\Delta T_{sub,o} = 4$ °C; c: $\Delta T_{sub,o} = 5$ °C.

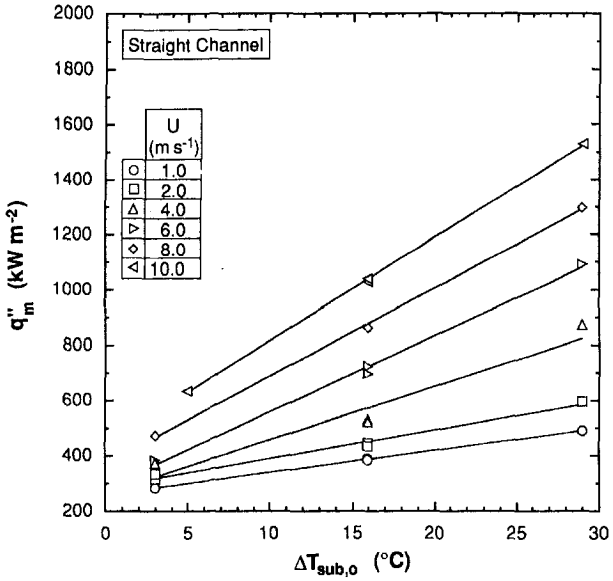

Fig. 5 Linear relationship between critical heat flux and outlet subcooling in straight channel

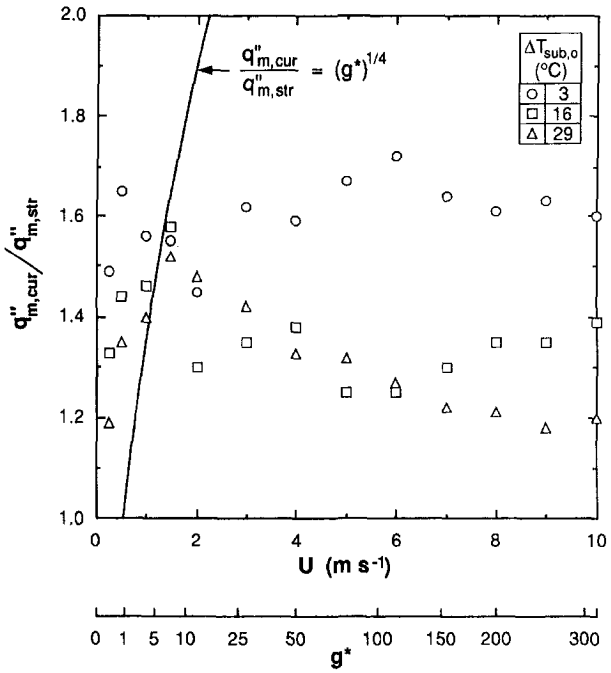

Fig. 7 Ratio of curved-to-straight-channel critical heat flux data versus velocity and centripetal acceleration at three subcoolings

several complex enhancement effects which are not reflected in the Zuber et al. model.

Enhancement Mechanisms

Figure 8 illustrates three key mechanisms for CHF enhancement in a curved channel: *buoyancy forces, additional pressure on liquid-vapor interface,* and *increase in wall subcooling,* all resulting from the radial pressure gradient.

The first mechanism is a buoyancy force which arises when matter that is less dense than its surroundings is in the presence of a pressure gradient. In this case, the force on a vapor bubble surrounded by the denser liquid pulls the bubble toward the inner wall. This results in a more efficient removal of vapor from the concave surface, making it less likely bubbles will coalesce on the heated surface and form a vapor blanket, as shown in Fig. 8(*a*). CHF is therefore delayed to higher fluxes where vapor production becomes so intense that coalescence outpaces vapor removal. Insight into the manner in which the buoyancy forces enhance CHF was obtained through flow visualization tests and will be discussed in the next section.

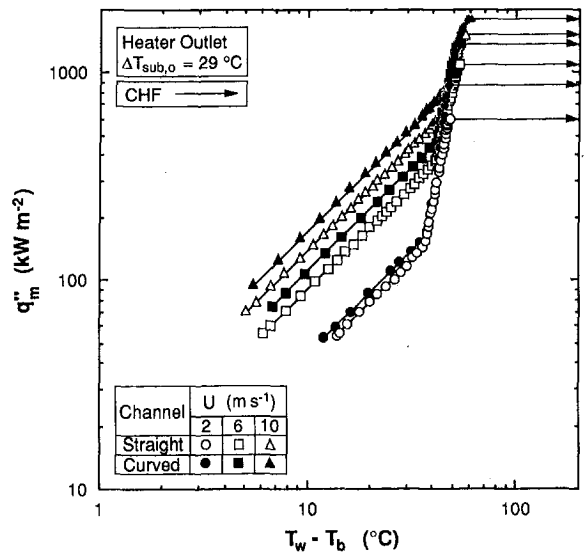

Fig. 6 Comparison of boiling curves at outlet of straight and curved heated sections for $\Delta T_{sub,o}$ = 29°C

Secondly, the pressure gradient enables the liquid contact with the wall, which occurs at wetting fronts (troughs) in the wavy liquid-vapor interface, to be maintained until higher fluxes, as illustrated in Fig. 8(*b*). Galloway and Mudawar (1993a, b) and Gersey and Mudawar (1995a, b) showed that CHF is triggered by lift-off of the liquid-vapor interface from the heated surface which occurs when the vapor momentum flux in the wetting front overcomes the pressure force exerted upon the wavy interface. The increase in pressure at the concave wall enables the liquid-vapor interface to withstand a greater vapor momentum which postpones lift-off to higher fluxes, thereby increasing CHF.

Thirdly, the radial pressure gradient increases the pressure and, consequently, the saturation temperature of the fluid at the concave wall, as indicated in Fig. 8(*c*). Compared to a straight channel, this leads to a local increase in subcooling which helps enhance CHF. This increase in subcooling may be estimated by making a few approximations. Pressure rise in a gravitational field is expressed by

$$\Delta P = \rho g h, \tag{4}$$

where ρ is the medium density, g the local acceleration, and h the change in position along the acceleration vector. The local acceleration in the curved channel may be approximated as the centripetal acceleration experienced by a fluid particle moving along the channel centerline (earth's gravity is neglected),

$$g \approx g_c = \frac{U^2}{\frac{1}{2}(R_1 + R_2)}. \tag{5}$$

For the sake of calculations, consider a straight and curved channel that have similar centerline pressures and bulk-averaged velocities. Fluid throughout the cross-section of the straight channel has the same pressure. But for curved flow, pressure increases at the concave wall, above that for straight flow, due to the gradient acting over half the channel height, i.e., $h = (R_2 - R_1)/2$. With these approximations, the pressure increase between the centerline and concave wall is given by

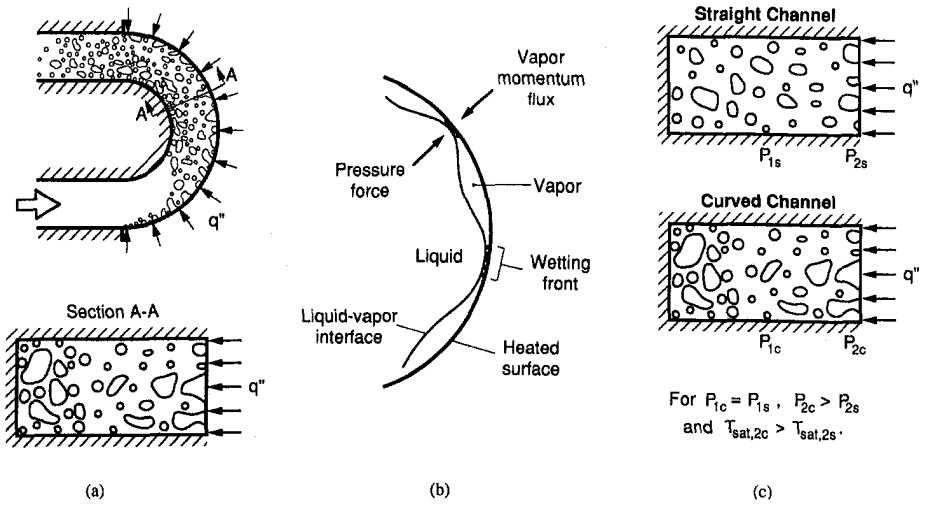

Fig. 8 Two-phase heat transfer enhancement mechanisms for flow boiling in a curved channel: (*a*) inward bubble motion due to buoyancy force, (*b*) increased pressure on liquid-vapor interface at wetting fronts, and (*c*) increased subcooling at wall

$$\Delta P = P_{2c} - P_{2s} = \rho_f U^2 \frac{R_2 - R_1}{R_1 + R_2}. \quad (6)$$

This represents the estimated increase in wall pressure between the curved and straight channels as a result of the radial pressure gradient, indicated in Fig. 8(*c*) as $P_{2c} - P_{2s}$. Using channel outlet pressure (P_o = 1.38 bar) as a reference point for saturation temperature, the increase in saturation temperature corresponding to this pressure increase can be determined using FC-72 property data. Assuming similar bulk temperatures between the two channels, this saturation temperature increase represents the increase in wall subcooling as well. Performing these calculations for $U = 10$ m s^{-1} reveals that the radial pressure gradient is responsible for a 3.2°C rise in subcooling. The associated rise in CHF may then be ascertained by referring to Fig. 5 which shows the linear relation between critical heat flux and subcooling in the straight channel. Extracting the slope for $U = 10$ m s^{-1} and multiplying by 3.2°C yields a CHF enhancement of 120 kW m^{-2} attributed to this radial increase in wall subcooling. This increment in critical heat flux represents only 32 percent of the enhancement measured for the near-saturated ($\Delta T_{sub,o}$ = 3°C) case and 40 percent for the highly subcooled ($\Delta T_{sub,o}$ = 29°C) case, at this velocity. This indicates that the other two mechanisms illustrated in Fig. 8 contribute significantly to the curvature enhancement. These issues are explored in the next section.

Flow Visualization Results

Equipment and Procedure. In order to gain insight into the relation between vapor dynamics and CHF, a visual investigation of the flow boiling process was undertaken. Two additional channels were fabricated from optical-grade polycarbonate (trade name Lexan MP750) with designs identical to those used in obtaining CHF data. Tests with these clear channels used the same heaters, instrumentation, fluid and flow loop, the only difference being optical access to the heated length.

A Canon L1 8-mm video camera was configured with its lens located a few millimeters above the channel. The camera was mounted on a tripod which enabled it to be translated in any coordinate direction and to traverse the entire heated length. Video sequences were recorded with a 30X lens at a rate of 30 frames per second and a shutter speed of 1/10,000 of a second. The view through the camera was parallel to the heated surface and perpendicular to the flow direction. Approximately 30 mm of the channel length were captured in a frame, so the 101.6-mm heated length was videotaped in four segments by traversing the camera.

For each flow visualization test, the heated length was videotaped for every heat flux increment (data point) of the boiling curve though only the vapor characteristics at CHF were measured and categorized. Video allowed for the collection of significantly more frames of vapor activity than could be acquired with still photography. This proved to be a tremendous asset in conducting the statistical analysis of vapor size, shape and percentage of occurrence.

Video sequences were obtained in both channels for only the near-saturated ($\Delta T_{sub,o}$ = 3°C) and highly subcooled ($\Delta T_{sub,o}$ = 29°C) cases for velocities of U = 0.25, 1, 2 and 4 m s^{-1}. Higher velocities were not attempted since vapor dimensions were approaching sizes too small to be measured reliably and since the integrity of the polycarbonate channels would be compromised at the higher heater temperatures associated with higher velocities. Small holes precisely spaced near the edge of the channel and captured in the video images provided a scale by which to make measurements of vapor dimensions. These measurements were obtained manually using a video monitor and a scale constructed for each test based on the known spacing of the small holes.

Flow Boiling Images. Composite video images of the straight and curved heated lengths, shown in Figs. 9 through 11, represent typical observations of vapor development along each channel. Channel height is 5.0 mm and width (depth of view into page) is 2.5 mm. The dark region along the channel edge is the heater (which is much thicker than actually shown) with upstream and downstream adiabatic sections of the channel revealed by the lighter shade. Thin dark lines that may be seen in some images are microcracks in the polycarbonate material which did not affect the boiling process. The small holes used as a measurement scale are visible along the edge of the channel.

Figure 9 shows flow boiling in the straight channel at CHF for near-saturated ($\Delta T_{sub,o}$ = 3°C) and subcooled ($\Delta T_{sub,o}$ = 29°C) conditions at a bulk velocity of U = 1 m s^{-1}. Flow is from left to right and the channel is flush with the heater at the inlet though the edge is not visible. These images clearly show vapor patches growing in both length and height. The larger patches restrict the access of liquid at high heat fluxes. Increasing subcooling reduces this restriction by decreasing vapor length and height as illustrated in Fig. 9(*b*). The series of vapor patches display an undulating, periodic nature which is the basis of the idealized wavy interface for CHF modeling first proposed by Galloway and Mudawar (1993a, b).

Vapor development at CHF in the curved channel is shown in Figs. 10 and 11 for near-saturated and subcooled conditions,

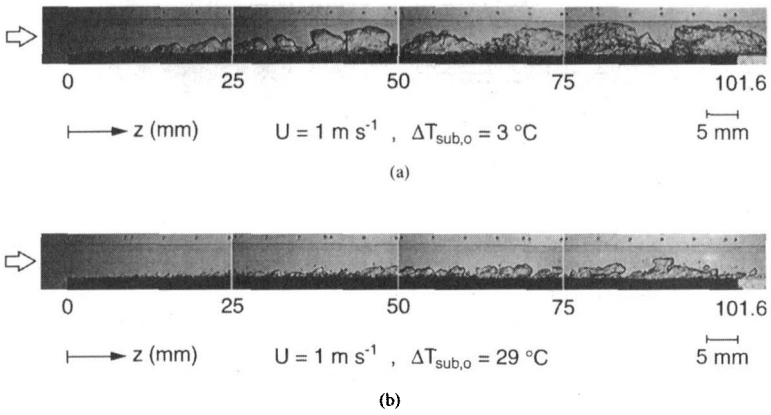

Fig. 9 Video images of flow boiling at CHF in straight channel at $U = 1$ m s^{-1} for (*a*) near-saturated ($\Delta T_{sub,o} = 3$°C) and (*b*) subcooled ($\Delta T_{sub,o} = 29$°C) conditions

respectively. Figure 10 shows a clear tendency of the buoyancy force to pull vapor inward removing it from the concave wall, especially near $z = 25$ mm where the vapor is being elongated and pinched. Farther downstream vapor exists throughout the cross section. It appears as though the buoyancy force pinches off a portion of the vapor mass that had formed along the concave wall and pulls this portion into the bulk. The result is numerous vapor fragments distributed throughout the cross section. Another consequence is that the vapor which does remain on the surface is not organized in large patches; this provides less resistance to the rewetting liquid. For subcooled flow, shown in Fig. 11, vapor production is significantly reduced but buoyancy can still be seen to act on small patches that are elongated toward the inner wall.

Comparing the near-saturated case of both the straight [Fig. 9(*a*)] and curved (Fig. 10) channels highlights the important effect of buoyancy forces. Vapor is removed from the concave wall, fragmented and distributed in the bulk flow where it is better able to condense, while in the straight channel it remains near the heated surface providing an impediment to the rewetting liquid. Also, the greater height of vapor patches near the inlet region in the curved channel are associated with a greater interfacial curvature at the wetting fronts, which results in a larger pressure difference across the interface. This pressure force acts to maintain liquid contact with the surface by more effectively resisting the vapor momentum flux, leading to an increased CHF. These phenomena are also present in the subcooled case where there is less vapor on the curved heated surface (Fig. 11) than on the straight [Fig. 9(*b*)] despite the fact that at the condition shown CHF is 40 percent greater in the curved channel.

Vapor Measurements. In an effort to quantify these observations, numerous near-wall vapor patches were measured in each channel at similar velocity and subcooling conditions. Particular characteristics of interest were vapor length, λ_{meas}, maximum height, δ_{meas}, and location of upstream edge, d_{up}, as illustrated in Fig. 12. Additionally, the length of liquid contact with the surface

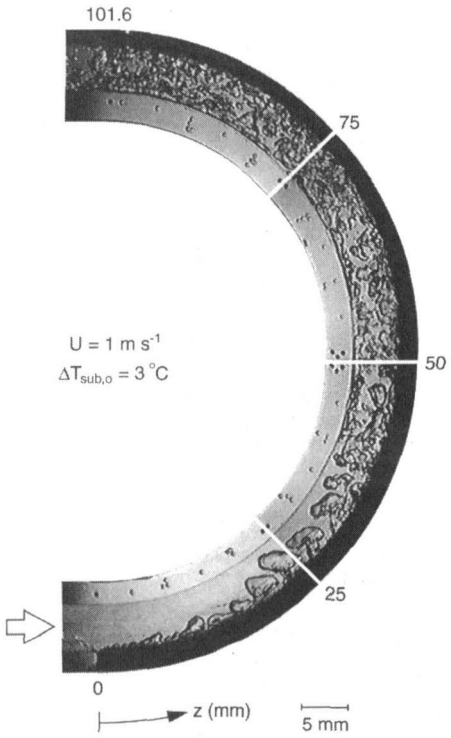

Fig. 10 Video images of flow boiling at CHF in curved channel at $U = 1$ m s^{-1} for near-saturated ($\Delta T_{sub,o} = 3$°C) conditions

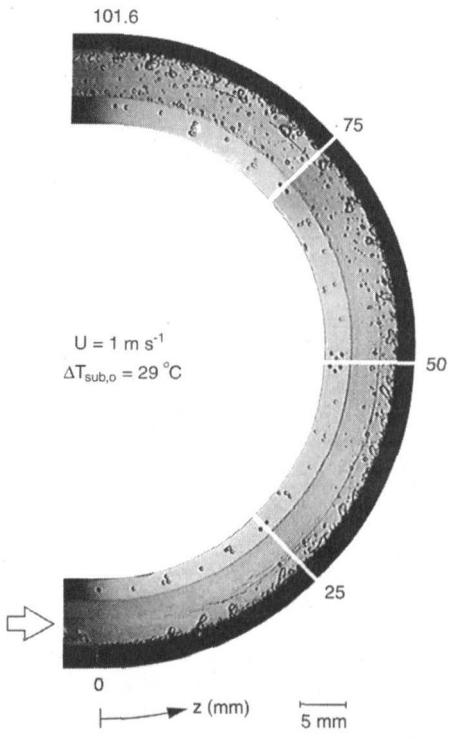

Fig. 11 Video images of flow boiling at CHF in curved channel at $U = 1$ m s^{-1} for subcooled ($\Delta T_{sub,o} = 29$°C) conditions

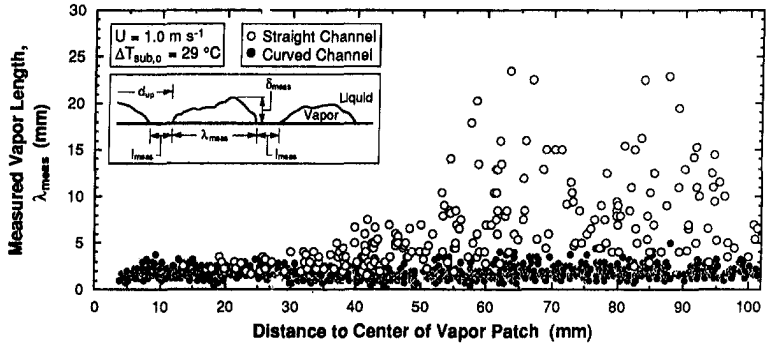

(a)

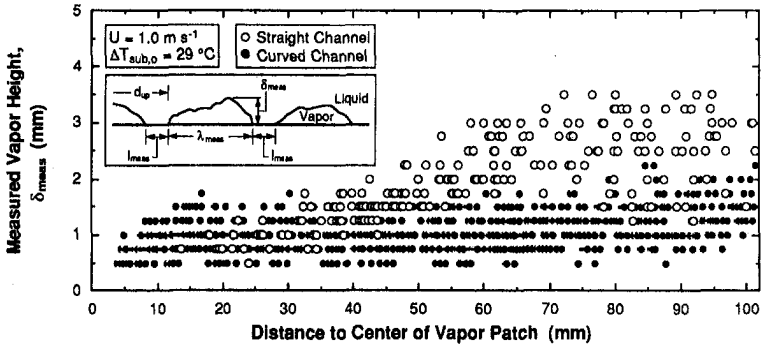

(b)

Fig. 12 Measured (*a*) lengths and (*b*) heights of vapor patches at CHF in straight and curved channels for $U = 1$ m s^{-1} and $\Delta T_{sub,o} = 29$°C

between adjacent patches, l_{meas}, was measured. In some cases, the identification of a vapor patch itself was difficult since boundaries were not always distinct. Considering the seemingly random nature of the boiling process, measurements were made on 50 video frames for each segment of the heater. In this manner, the bubble dynamics could be analyzed statistically to identify characteristics that might not be apparent in a few frames.

The measurements were analyzed individually by plotting them versus streamwise location and collectively by averaging values for each of the four heater segments. In general, the data show that for straight channel flow the vapor length, vapor height, and liquid length all increase along the flow direction, decrease with increasing subcooling, and decrease with increasing velocity. The liquid and vapor lengths vary such that their ratio is relatively constant for a given subcooling. For curved flow, vapor length and height do not grow downstream, instead they assume relatively constant values.

The effect of curvature on vapor length is ascertained by plotting the measured length of a vapor patch against the distance to the center of that vapor patch as measured from the heater inlet. Measurements made for the straight and curved channels are shown in Fig. 12(*a*) for conditions of $U = 1$ m s^{-1} and $\Delta T_{sub,o} = 29$°C. The vapor length grew downstream in the straight channel (albeit with scatter) whereas it remained at a lower, constant value in the curved channel. This is a direct consequence of the buoyancy forces present in the curved flow. These forces pull the vapor inward, eventually breaking off a portion of the patch such that the vapor remaining on the surface is reduced in length and height. Buoyancy continues to act along the entire curved trajectory preventing the vapor mass from growing significantly.

An illustration of attenuated vapor height in curved flow is given in Fig. 12(*b*) for $U = 1$ m s^{-1} and $\Delta T_{sub,o} = 29$°C. The vapor height increased downstream in the straight channel but remained fairly constant in the curved. Of particular interest is the upstream region (0–25 mm) of both heaters where CHF is believed to be triggered due to wetting front lift-off. The plot shows that vapor height in this region is greater in the curved channel. Buoyancy forces pull vapor patches inward, elongating them in the radial direction, such that their heights measured normal to the heated surface are greater than at corresponding locations in the straight channel. Shortly downstream though, buoyancy forces pinch off portions and the heights of the vapor patches remaining on the curved surface are less than on the straight surface. This is particularly evident by comparing the video images for the near-saturated case in Figs. 9(*a*) and 10. With respect to Fig. 12(*b*), the "row-effect" displayed by the data is merely a consequence of making vapor measurements to the nearest 0.25 mm.

Vapor Shape Analysis. In addition to obtaining measurements, the vapor patches were categorized based on shape to identify characteristics pertinent to CHF. These categories are depicted in Fig. 13. By far the most common form observed was the generic wave-like shape with no special features. It was typically a vapor mass with maximum thickness near its center and tapered on the ends. This wave-like formation, depicted in Fig. 13(*a*), grows by the addition of newly generated vapor and by coalescence with other vapor masses.

Two other shapes that warrant discussion highlight the forces acting on the vapor. The overhanging vapor type, shown in Fig. 13(*b*), was observed almost exclusively in the straight channel though far less frequently than the wave-like type. This formation is initiated with vapor generated at the heated surface. The momentum of the newly created vapor is directed away from the wall toward the center of the channel where the local velocity is greater. The liquid momentum in the middle of the channel moves the vapor in the streamwise direction while its base maintains contact

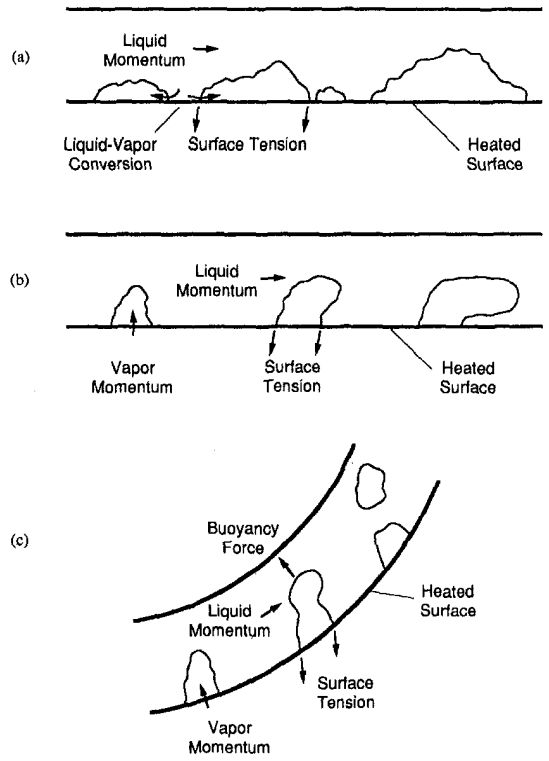

Fig. 13 Vapor formations observed in straight and curved channels: (*a*) wave-like, (*b*) overhanging, and (*c*) pinching

with the wall through surface tension forces, creating the overhanging formation. Once the trapped liquid is evaporated, rewetting of the surface by the cooler bulk is hindered by the interference of the overhanging vapor.

The pinching type formation illustrated in Fig. 13(*c*) was observed chiefly in the curved channel. Similar to the overhanging formation, it too is initiated by vapor generated at the surface and thrust outward due to its momentum. Streamwise inertia acts to push it along the flow while a buoyancy force provides the distinguishing effect. This buoyancy force pulls the vapor toward the inner wall elongating it in the radial direction. Eventually, portions of the vapor are pinched off with the fragmented portions being pulled toward the inner wall. Unlike in the straight channel where the large, overhanging vapor remains near the surface hindering the liquid rewetting, in the curved channel this vapor is moved away from the surface toward the opposite wall. This pinching behavior is evident in Fig. 10 near $z = 25$ mm.

These two vapor formations illustrate an important distinction between straight and curved channel flow boiling that is a major contributor to the CHF enhancement. In both cases, vapor is generated at the wall while surface tension and streamwise inertia act to maintain it there. However, the radial pressure gradient present in curved flow leads to buoyancy forces which move vapor away from the concave wall.

Statistical results reveal that the dominant vapor shape is that of the wave-like formation. The overhanging vapor formation occurred mostly in the straight channel typically less than ten percent of the time. However, for subcooled flow at $U = 1$ m s^{-1}, it represented nearly one quarter of the observed patches over the downstream half of the heater. The pinching formation appeared only in the curved channel due the buoyancy forces pulling on the vapor. It also was observed less than ten percent of the time except at $U = 1$ m s^{-1} for $\Delta T_{sub,o} = 29$°C where it was noted up to 20.4 percent of the time.

Effects of Buoyancy Mechanism. The flow visualization results, both the qualitative observations and the quantitative measurements, along with the CHF data permit several conclusions to now be drawn regarding the effects of buoyancy on CHF.

First, near-saturated flow realizes a greater benefit from flow curvature. The experimental data plotted in Fig. 7 show that the critical heat flux enhancement ratio is greatest for the lowest subcooling. The vapor generated in near-saturated flow does not readily condense and hence must be removed from the surface. The buoyancy forces arising from the radial pressure gradient aid in removing this vapor thereby delaying coalescence and CHF. On the other hand, highly subcooled flow is already very efficient at removing vapor from the heated wall by condensing it in the cooler bulk. Hence, the effect of an additional mechanism such as that provided by a buoyancy force is less significant in highly subcooled flow. Therefore, curvature has a more pronounced enhancement effect for near-saturated flow.

Secondly, curved flow better utilizes the available subcooling of the bulk flow. As clearly shown in Fig. 10, buoyancy forces break off portions of surface vapor patches and move these smaller portions into the cooler bulk flow where they condense. In this manner, the subcooling throughout the cross-section is available for condensing the vapor. Additionally, condensation is aided by the fact that there are numerous small, jagged patches in the bulk. This greatly increases the surface area available for the transfer of heat from saturated vapor to subcooled liquid as compared to the vapor remaining in large patches, typical of straight channel flow.

Thirdly, the buoyancy mechanism aids in providing the bulk liquid greater access to the concave wall. Buoyancy forces pull vapor away from the wall attenuating the length and height of vapor remaining on the surface. This counters the continual coalescence and restriction that occur as vapor is advected downstream, as in the straight channel. The flow boiling images in Fig. 10 and the vapor measurements in Fig. 12 illustrate that the buoyancy forces continually pinch off portions of the vapor. Consequently, the smaller surface vapor patches result in greater access for the rewetting liquid and a corresponding increase in heat transfer; hence, a higher CHF limit in the curved channel.

Finally, curvature of the liquid-vapor interface is greater for curved flow. The buoyancy forces pull on the surface vapor patches elongating them in the radial direction. This elongation takes place over the upstream region before the forces become strong enough to break off portions and pull them into the bulk. Figure 12(*b*) shows that the individually measured vapor heights are larger in the curved channel over approximately the first 25 mm. Consequently, the amplitude of the vapor wave is larger resulting in greater interfacial curvature. This leads to a larger interfacial pressure difference which is able to withstand a greater vapor momentum flux, thereby maintaining liquid contact with the surface at higher fluxes, increasing CHF. This interfacial pressure difference plays a significant role in the lift-off criterion of the critical heat flux model first proposed by Galloway and Mudawar (1993b).

Conclusions

This paper details an investigation into critical heat flux enhancement resulting from streamwise curvature in a rectangular concave-heated channel. Test were conducted in curved and straight channels to obtain CHF data and to visualize the corresponding vapor characteristics. Key conclusions from this study are as follows:

1 Critical heat flux increases with increasing velocity and subcooling for both straight and curved flow. CHF increases linearly with outlet subcooling in straight flow but does not show a consistently linear relationship in curved flow.

2 For all flow conditions tested, curvature augments the critical heat flux limit. At high velocities, this augmentation is approximately 60 percent for $\Delta T_{sub,o} = 3$°C, 40 percent for $\Delta T_{sub,o} = 16$°C, and 20 percent for $\Delta T_{sub,o} = 29$°C. Clearly, the enhancement in CHF is better realized at low subcooling where the flow is more dependent upon the buoyancy force for vapor removal.

3 Prior to CHF, vapor bubbles in both channels coalesce into a wavy vapor layer consisting of vapor patches which propagate downstream along the heated wall. Vapor patch length and height grow along the flow direction and decrease with increasing velocity and subcooling in the straight channel. An additional overhanging vapor formation was observed in the straight channel while a pinching formation occurred in the curved channel. The distinguishing factor between these latter two is attributed to buoyancy forces pulling the vapor toward the inner wall in the curved channel. The buoyancy forces elongate, then pinch off portions of the vapor patches in the curved channel; these fragmented portions are pulled into the bulk flow. As a consequence, vapor length and height are smaller at most locations in the curved channel and do not increase in the flow direction.

4 The key mechanisms for CHF enhancement in curved flow can be summarized as follows:

(a) Radial increase in pressure leads to a higher local subcooling at the concave wall.

(b) Buoyancy forces pull vapor away from the concave wall thereby delaying coalescence and providing the rewetting liquid greater access to the heated surface.

(c) Buoyancy forces pinch off and transport portions of the vapor into the cooler bulk. In this way, curved flow is better able to utilize the available subcooling throughout the cross section.

(d) Buoyancy forces pull on the surface vapor patches elongating them in the radial direction. This results in a larger pressure difference across the liquid-vapor interface which acts to maintain liquid contact with the surface by more effectively resisting the vapor momentum flux, leading to an increased CHF.

Acknowledgments

The authors are grateful for the support of the Office of Basic Energy Sciences of the U.S. Department of Energy (Grant No. DE-FG02-93ER14394.A003). Financial support for the first author was provided through the Air Force Palace Knight Program.

References

Collier, J. G., and Thome, J. R., 1994, *Convective Boiling and Condensation,* 3rd Ed., Clarendon Press, Oxford.

Gambill, W. R., and Green, N. D., 1958, "Boiling Burnout with Water in Vortex Flow," *Chemical Engineering Progress,* Vol. 54, pp. 68–76.

Galloway, J. E., and Mudawar, I., 1993a, "CHF Mechanism in Flow Boiling From a Short Heated Wall—Part I. Examination of Near-Wall Conditions with the Aid of Photomicrography and High-Speed Video Imaging," *International Journal of Heat and Mass Transfer,* Vol. 36, pp. 2511–2526.

Galloway, J. E., and Mudawar, I., 1993b, "CHF Mechanism in Flow Boiling From a Short Heated Wall—Part II. Theoretical CHF Model," *International Journal of Heat and Mass Transfer,* Vol. 36, pp. 2527–2540.

Galloway, J. E., and Mudawar, I., 1995, "A Theoretical Model for Flow Boiling CHF From Short Concave Heaters," ASME JOURNAL OF HEAT TRANSFER, Vol. 117, pp. 698–707.

Gersey, C. O., and Mudawar, I., 1995a, "Effects of Heater Length and Orientation on the Trigger Mechanism for Near-Saturated Flow Boiling Critical Heat Flux—I. Photographic Study and Statistical Characterization of the Near-Wall Interfacial Features," *International Journal of Heat and Mass Transfer,* Vol. 38, pp. 629–641.

Gersey, C. O., and Mudawar, I., 1995b, "Effects of Heater Length and Orientation on the Trigger Mechanism for Near-Saturated Flow Boiling Critical Heat Flux—II. CHF Model," *International Journal of Heat and Mass Transfer,* Vol. 38, pp. 643–654.

Gu, C. B., Chow, L. C., and Beam, J. E., 1989, "Flow Boiling in a Curved Channel," *Heat Transfer in High Energy/High Heat Flux Applications,* R. J. Goldstein, L. C. Chow, and E. E. Anderson, eds., ASME, New York, ASME HTD-Vol. 119, pp. 25–32.

Hughes, T. G., and Olson, D. R., 1975, "Critical Heat Fluxes for Curved Surfaces During Subcooled Flow Boiling," *U.S. National Heat Transfer Conference,* Vol. 3, San Francisco, CA, ASME, New York, pp. 122–130.

Leland, J. E., and Chow, L. C., 1992, "Effect of Channel Height and Radius of Curvature on Forced Convective Boiling in a Rectangular Channel," *30th Aerospace Sciences Meeting & Exhibit,* Reno, NV.

Wu, P. S., and Simon, T. W., 1994, "Critical Heat Flux and Subcooled Flow Boiling with Small Heated Regions on Straight and Concave-Curved Walls," *10th International Heat Transfer Conference,* Institute of Chemical Engineers, Rugby, UK, Vol. 7, pp. 569–574.

Wu, P. S., and Simon, T. W., 1995, "Subcooled Flow Boiling Over a Thin, Low-Capacitance Surface on a Concave Wall," *ASME National Heat Transfer Conference,* Portland, OR, Vol. 12, pp. 177–184.

Zuber, N., Tribus, M., and Westwater, J. M., 1961, "The Hydrodynamic Crisis in Pool Boiling of Saturated and Subcooled Liquids," *International Developments in Heat Transfer: Proceedings of the 1961–62 International Heat Transfer Conference,* Boulder, CO, ASME, New York, pp. 230–236.